Proceedings of the
International Conference on Mechanical Engineering 2007
(ICME2007) 29- 31 December 2007, Dhaka, Bangladesh

ICME07-TH-24

ANALYSIS OF STEADY TESTS FOR POST-BT HEAT TRANSFER IN VERTICAL TUBE GEOMETRY IN ABNORMAL OPERATIONAL TRANSIENTS OF BWRS

M. S. Islam[1], Y. Sibamoto[2], Y. Maruyama , H. Nakamura and M.A. Zulquarnain[1]

[1]Bangladesh Atomic Energy Commission, Dhaka, Bangladesh
[2]Thermohydraulic Safety Research Laboratory . Nuclear Safety Research Center, Japan Atomic Energy Agency (JAEA), 2- 4 Shirakata shirane, Tokaimura, Nakagun, Ibaraki, Japan

ABSTRACT

Comparative studies among the experimental, numerical and empirical on steam-water two-phase heat transfer characteristics in the post boiling transition (post-BT) region were carried out in a vertical tube with a diameter of 12.2 mm under mass fluxes from 300-800 kg/m^2.s for a particular operating pressure of 2 MPa at steady state condition. Numerical analysis was performed using a subchannel code, COBRA-TF to understand the code characteristics and the predictive capability for the BT and post-BT heat transfer by comparing numerical results with steady state single-tube experimental data during anticipated operational transients. Both the experimental and numerical studies have shown that the post-BT heat transfer strongly depends on the wall superheat. The local heat transfer coefficient is high in the low wall superheat region and decreases with an increase in the wall superheat asymptotically. The enhancement of heat transfer coefficient is not expected with the increase of mass flux and operating pressure as well. The agreement between experimental and numerical results is well specially in the high wall superheat condition than that of the low wall superheat condition. Among the three referred post-BT empirical correlations, Koizumi's correlation for multi rod geometry instead of single rod well simulates the experimental heat transfer data both in the high and low wall superheat conditions. The data and results can be used not only to develop a mechanistic or phenomenological model but also to assess the predictive capability of the existing empirical correlations for simulating abnormal operational transients in the fuel assemblies of Boiling Water Reactors (BWRs).

Keywords: Template, Typing Instruction, Double column.

1. INTRODUCTION

In order to secure fuel integrity, Light Water Reactors (LWRs) cores are designed to avoid the onset of boiling transition (BT) inside the fuel assembly that leads to deterioration of heat transfer and subsequent excessive rise of fuel cladding temperature during anticipated abnormal operational transients that might occur in a power plant. Based on the recent extension of technical know-how, however, the Atomic Energy Society of Japan issued "Standard for Assessment of Fuel Integrity under Anticipated Operational Occurrences in BWR Power Plants" [22], which allows BT to occur during anticipated abnormal transients of BWRs. The standard describes an allowable level of thermal loads imposed on fuel cladding, and a predictive methodology for the thermal loads represented by cladding temperature and duration of cladding dryout. The thermal loads on fuel cladding could be controlled by thermal power at the BT onset, post-BT heat transfer between fuel cladding and surrounding coolant, and rewetting of dryout region of cladding. In order to apply the standard into a governmental regulation process, the predictive methodology for the thermal loads on fuel cladding must be assessed to be technically appropriate. As one of advanced uses of existing LWRs, it is expected that the uprate of core thermal power is introduced in near future. The power uprate could result in decreasing a margin to the onset of BT. Thus, a phenomenologically reliable methodology for prediction of the BT onset is needed. Additionally, post-BT thermal behavior of fuel cladding should be well understood in order to more realistically assess the integrity of fuel cladding during anticipated operational transients.

With the background mentioned above, a series of experiments with detailed measurement instrumentation is presently underway at Japan Atomic Energy Agency (JAEA) for upgrading database on BT and post-BT behavior [11]. The database is applied not only for the development of mechanistic models but also for the assessment of predictive capability of existing empirical correlations. Many empirical correlations have been proposed for the onset of BT, post-BT heat transfer and rewetting with different levels in consideration of physics related to the phenomena [3, 4, 15]. Those correlations are generally simple in use but have a limited range of validity.

Analytical codes for thermal-hydraulics can be used to evaluate water vapor two-phase flows in reactor cores including BT and post-BT phenomena. Especially, a subchannel code is a valuable tool for detailed analysis of thermal-hydraulics in fuel bundles of BWR cores during design basis accidents and anticipated abnormal transients. One of the major objectives of the present study is to assess the predictive capability of a subchannel code, COBRA-TF, for the BT onset and post-BT heat transfer by comparing analytical results with steady-state single-tube experimental data at JAEA performed under a pressure of 2 MPa and a mass flux range of 300-1200 kg/m^2.s. The authors are also attempted to assess widely used empirical correlations through comparison with post-BT heat transfer data in the same experiments. A brief description of the experimental set up and its procedures are given in **C**hapt.2 Numerical analysis of the experimental data for the BT onset and post-BT heat transfer characteristics is provided in Chapt.3. Chapt.4 includes the results and discussions of the tests, numerical and referred empirical post-BT correlations while Chapt. 5 draws the concluding remarks of the present investigation

2. EXPERIMENTAL SET UP AND PROCEDURE

A single vertical tube post-BT test facility was used. The flow cross-sectional area of the test facility was circular which simulated that of a BWR subchannel flow. Schematic diagram of the experimental loop is presented in Fig. 1. The preheating and test sections were 3.0 and 0.5 m long, respectively, whose inner diameter was 12.2 mm with a wall thickness of 2.3 mm. These two sections were fixed one after another. It was possible to place a droplet deposition section between preheating and test sections, or at the exit of the test section. A length of the deposition section was chosen from 0.5, 1.0 or 1.5 m. The tube was made of Incoloy and it was electrically heated uniformly by direct current.

In steady test series, stepwise power supply was initially made on the preheating section under specified conditions of pressure and water flow rate. After confirming an increase of the tube wall, corresponding to liquid film dryout, at the exit location of the preheating section (BT-condition), the stepwise power supply was stopped. Then stepwise power was started to supply to the test section. The wall temperature of the preheating and test sections was monitored by the thermocouple reading and then recorded in a data acquisition system. Total thirty three chromel-alumel thermocouples of 1 mm diameter were embedded on the tube outer wall surface.

Figure 2 shows a conceptual view of the occurrence of liquid film dryout at the preheating and test sections for a particular flow rate condition and heat flux to the liquid flow. The liquid film on the inner wall of the test section was formed by the deposition of liquid droplets denerated in the preheating section. Stepwise direct heat (q_1) was supplied first to the preheating section until dryout occurs and then stepwise direct heat (q_2) was supplied to the test section further occurring dryout in the heated test section. Twelve thermocouples were embedded in the left side and another twelve were embedded in the right side of the test section. Seven thermocouples were embedded in the preheating section. The data from these thermocouples were used to detect the onset of the liquid film dryout and to evaluate heat transfer coefficients at the inner wall of the test section.

The slightly subcooled demineralized water flowed up into the entrance region of the preheating section and then passed into the test section. The temperature of the incoming water was controlled by the preheater with the maximum power of 30 kW. The system pressure was controlled by the pressurizer. The flow rate was controlled by the flow control valve. The water-vapor two-phase fluid in downstream of the test section was returned to the pressurizer and then recirculated into the preheating section by the circulation pump after proper mixing of the liquid in the mixing chamber.

3. BRIEF DESCRIPTION FOR NUMERICAL ANALYSIS

3.1 Numerical Scheme and Governing Equations

COBRA -TF code (reference) provides a two-fluid, three-field representation of two-phase flow with either rectangular Cartesian or subchannel coordinates of eight conservation equations; six equations of mass and momentum conservation for continuous liquid, continuous vapor, and entrained liquid drop fields, and two equations of energy conservation for liquid and vapor phases. Each field is treated in three dimensions in subchannnel coordinate and is compressible. The conservation equations and heat conduction within the solid structures in contact with the fluid are solved using a semi-implicit, finite-difference numerical technique on an Eulerian mesh. The velocities are obtained at mesh cell faces, and the state variables (e.g., pressure, density, enthalpy and phasic volume fractions) are obtained at the cell center.

The conservation of mass equation is as follows;

$$\frac{\partial}{\partial t}(\alpha_k \rho_k) + \nabla.(\alpha_k \rho_k U_k) = \Gamma_k \quad (1)$$

The conservation of momentum equation is as follows;

$$\frac{\partial}{\partial t}(\alpha_k \rho_k U_k) + \nabla.(\alpha_k \rho_k U_k U_k) = \alpha_k \rho_k g - \alpha_k \nabla P + \nabla.\left[\alpha_k (\tau_k + \overset{T}{T}_k)\right] + \overset{\Gamma}{M}_k + \overset{d}{M}_k \quad (2)$$

The conservation of energy equation is as follows;

$$\frac{\partial}{\partial t}(\alpha_k \rho_k H_k) + \nabla.(\alpha_k \rho_k H_k U_k) = -\nabla.\left[\alpha_k (Q_k + \overset{T}{Q}_k)\right] + \Gamma_k \overset{i}{H}_k + q'''_{ik} + \alpha_k \frac{\partial P}{\partial t} \quad (3)$$

A set of constitutive equations for heat transfer, mass transfer and momentum exchange is explicitly coupled as source terms to the governing equations in order to predict the thermal-hydraulic behavior.

The heat transfer package consists of a set of heat transfer correlations and a selection logic algorithm. When void fraction is larger than 0.9, a dispersed film flow is selected, in which the Dittus-Boelter correlation (reference) is used for vapor single-phase

The heat transfer package consists of a set of heat transfer correlations and a selection logic algorithm. When void fraction is larger than 0.9, a dispersed film flow is selected, in which the Dittus-Boelter correlation (reference) is used for vapor single-phase convection as

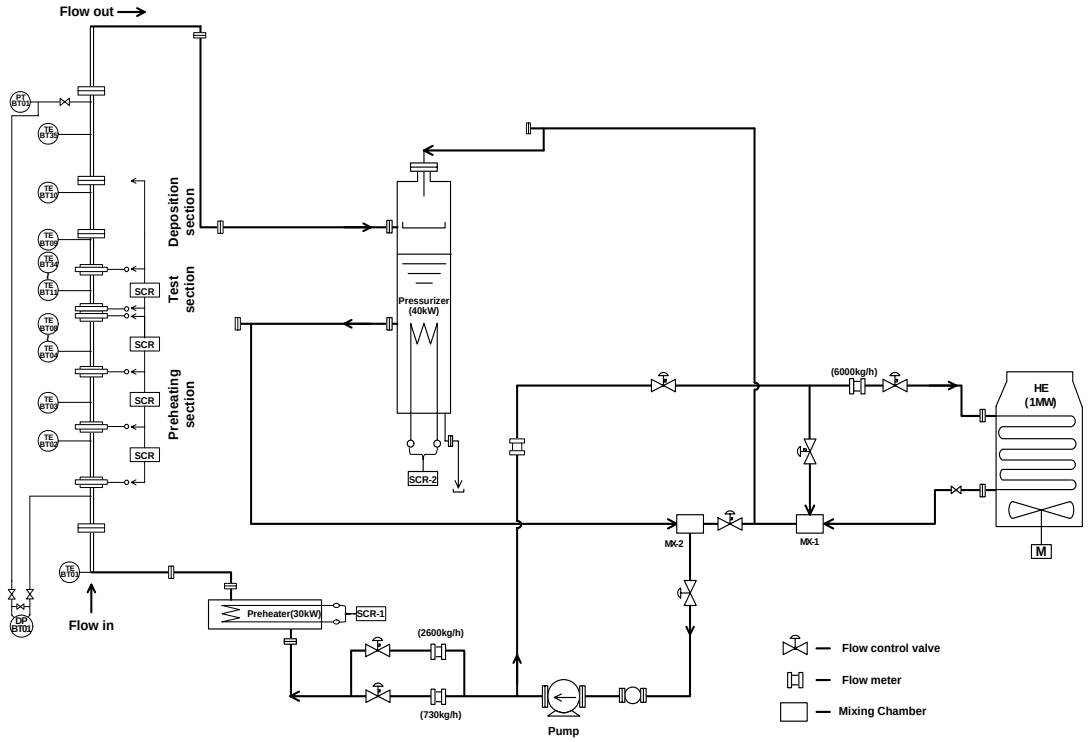

Fig 1: Flow diagram of test loop

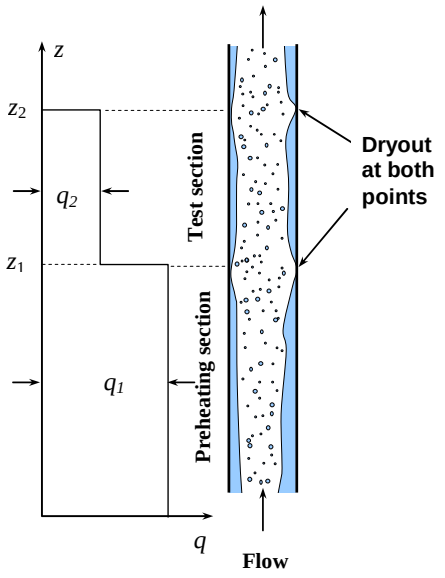

Fig 2: Schematic diagram of the dryout point at preheating and test sections under variable heat flux conditions

a dominant heat transfer mode. This model has an important role in prediction of post-BT heat transfer. The equation is presented as;

$$h_{D-B} = 0.023 \frac{\lambda}{D_H} \left(\frac{G \times D_H}{\mu} \right)^{0.8} \mathrm{Pr}^{0.4} \qquad (4)$$

The physical properties are taken at film temperature. Radiative heat transfer from hot wall to vapor and to liquid droplets, in addition to direct contact of liquid droplets onto the wall, are taken into account in post-BT heat transfer calculation. Several physical models related to entrainment and deposition of liquid droplets are prepared in COBRA-TF code as mass transfer constitutive equations. In the present numerical analysis, the following models on entrainment and deposition were applied.

i. Wurtz's entrainment model (reference)

The liquid entrainment rate, m_E is calculated as follows:

$$m_E = 0.42 \left(\frac{k_s \times \tau_i}{\sigma} \right) \left(\frac{u_g \times u_l}{\sigma \times g} \right) P_w \times \Delta X \qquad (5)$$

ii. Sugawara's droplet deposition model (reference)

Droplet deposition rate, m_D is expressed as follows:

$$m_D = k_D \times C \qquad (6)$$

Droplet deposition coefficient, k_D is written as;

$$k_D = 0.009 \times u_g \left(\frac{C}{\rho_g} \right)^{-0.5} \mathrm{Re}_g^{-0.2} \times Sc^{-2/3} \qquad (7)$$

Where, Re_g and Sc are the gas phase Reynolds number and the Schmidt number, respectively.

3.2 Initial and Boundary Conditions

Initial and boundary conditions for the actual test component consist of initial system operating conditions, boundary conditions on individual computational cells within the model geometry. The initial system operating conditions define the state of the model component at the beginning of the transient and consist of system pressure, fluid enthalpy, mass flux into the system, and the average power generation rate,

expressed as an average linear heat rate. The initial pressure and enthalpy are used to determine the initial properties of the fluid in the channel. The channel data such as nominal flow area, wetted perimeter, tube wall thickness or inside diameter, the average linear heat generation rate per active rod shall be provided as an input data to simulate the test conditions. Two main types of boundary conditions such as inlet and outlet conditions on channel, and specific boundary conditions on particular cells within the mesh for both the vertical and transverse control volumes can be specified by input. Mesh cell boundary conditions may be applied wherever needed, on any face of any cell within the model geometry. The specified boundary values are pressure and enthalpy or flow rate and enthalpy, either or both of them can be changed with time by forcing function tables.

3.3 Description of Input

To analyze with COBRA-TF code, only the preheating, test and deposition sections were modeled in a single subchannel treatment with some appropriate boundary conditions given at the inlet of the preheating section and the outlet of the deposition section. That is, the total mass flow rate and the fluid enthalpy are given at the inlet and the pressure is given at the outlet. The steam quality at the inlet is determined based on the enthalpy of the entering water. The channel noding diagram employed in the present calculations is given in Fig. 3. It consists of 140 nodes; 100 of the same size where each node is 0.03 m high in the preheating section, 20 nodes of the same size both in the test and deposition sections where each node is 0.025 m high. The inner and outer diameters are 0.0122 and 0.0168 m, respectively. Calculation time was set to be 30s so as that a steady state condition was obtained. Calculation results tended to approach to the conversed values within this calculation time.

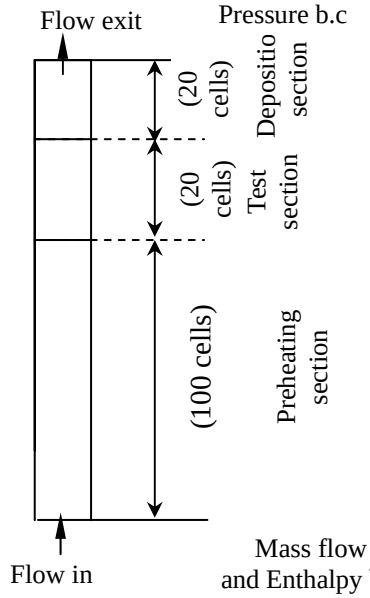

Fig 3: Noding diagram of numerical analysis with COBR-TF code

4. RESULTS AND DISCUSSIONS

Increasing heat input to the preheating section will lead to liquid film dryout that causes significant rise in wall temperature of the section. The dryout point is defined in the present analysis when liquid volume fraction is less than or equal to 0.001. The defined dryout was confirmed near the top-end preheating test section under the constant mass flux and operating pressure conditions. In the experiments, uniform direct electrical power was increased step by step. Power supply was stopped when there was a sudden rise in outer wall temperature of the preheating section which corresponds to critical power at the preheating section. The uncertainty in the temperature measurement was less than 1.5% at the most. Figure 4 shows the comparison of critical linear power density between the observation and the calculation with COBRA-TF code in the preheating test section under the mass fluxes of 300-1200 kg/m^2.s and operating pressure range of 2-7 MPa. It has found that the calculated critical linear power density agreed well with the observation with a maximum deviation of ± 5%.

After confirmation of the dryout occurrence in the preheating section, then stepwise direct electrical power was started to supply to the test section. Under different heat inputs on the test section, vertical profiles of the outer wall temperature were recorded and compared with the predicted results done by the present analysis. Figure 5 (TS01 to TS03) shows the calculated and measured outer wall temperature at mass fluxes of 300-800 kg/m^2.s for an operating pressure of 2MPa. The boiling mode is still nucleate boiling and the outer wall temperature is sustained at near the saturation temperature in the upstream part of the test section in the tests. Due mainly to the evaporation and droplet entrainment from the liquid film, the dryout occurs at certain locations leading the increase of the wall temperature. As shown in Fig. 5 (TS01) as an example, at larger linear power density (11 kW/m), the dryout occurs at lower locations than the smaller linear power density (8.32 kW/m) at the same mass flux of 300 kg/m^2.s and operating pressure of 2MPa.

The numerical analysis with COBRA-TF code can not reproduce the wall temperature profile of the test section observed in the tests. At higher mass flux of 500 kg/m^2.s, dryout occurs slowly at the two linear power levels which are shown in Fig. 5 (TS02). This is because of the higher mass flux effect even though higher linear power was given to the higher mass flux of 500 kg/m^2.s than that of the lower mass flux of 300 kg/m^2.s under the same operating pressure. However further increase of mass fluxes from G=500 to 800 kg/m^2.s, location of dryout point shifts a little downward which is shown in Fig. 5 (TS03). Increase of higher mass flux shows the increase of surface temperature with the increase of linear power supply over the heated tube. This tendency has been confirmed both the numerical analysis and the test data. At higher mass flux of 800 kg/m^2.s, the predicted surface temperature by the COBRA-TF code seems to be come closer to the test value.

Local heat transfer coefficients are derived in the

tests from the heat input and the inner wall temperature, which is estimated from the measured outer wall temperature of the test section, as given below:

$$h_{\exp} = \frac{q_w}{T_w - T_{sat}} \tag{8}$$

In the numerical analysis, heat transfer coefficients for the post-BT region are basically obtained from the Dittus-Boelter correlation, taking into account effects of radiation and direct heat transfer to deposited droplets. Figure 6 (TS01) shows the local heat transfer coefficient as a function of wall superheat in case that the vapor quality (x_1) of flow at the inlet of the test section is 0.94. The plot reveals that higher heat transfer coefficient is found in the lower wall superheat region and heat transfer coefficient decreases with increasing wall superheat. The enlargement of heat transfer coefficient in the low wall superheat region corresponds to nucleate or transition boiling. On the other hand, heat transfer is deteriorated in the high wall superheat region due to liquid film dryout for dominating vapor core over the heated surface. The same trend is revealed from the numerical prediction performed by COBRA-TF code and match well with the experimental heat transfer data in the higher wall superheat region and a large scatter prediction is found in the lower superheat region.

The heat transfer coefficient obtained from Koizumi, modified Dougall-Rohsenow, and Groeneveld correlations (references) in the post-BT region are also plotted in Fig. 6 (TS01).

Koizumi's correlations for multi rods and single rod geometries are figured out in Eq. (9) and Eq. (10), respectively:

$$\frac{h}{h_G} = (C_1 P + C_2)\ \exp\left(-\frac{T_w - T_s}{C_3 P + C_4}\right) + C_5 \tag{9}$$

where, $C_1 = 0.81$, $C_2 = 9.7$, $C_3 = -1.7$, $C_4 = 31$, $C_5 = 1.2$. The Koizumi's correlation for multi rods is valid for mass fluxes from 15 to 600 kg/m^2.s, qualities from 0.75 to 1.0, wall superheat from 25 to 325 K and operating pressures from 3 to 12 MPa.

$$\frac{h}{h_G} = (C_1 x_1 + C_2)\ \exp\left(-\frac{T_w - T_s}{C_3 x_1 + C_4}\right) + C_5 \tag{10}$$

Where, $C_1 = -35$, $C_2 = 42$, $C_3 = -35$ K, $C_4 = 66$ K, $C_5 = 1.5$.

The only difference between Koizumi's correlation for single rod and multi rods is the operating pressure. The experiments, on which the correlation for single rod based, was conducted only at an operating pressure of 3MPa under the same mass fluxes, qualities, and wall superheat conditions. Data utilized in developing correlation for a single rod based covered mass fluxes from 100 to 310 kg/m^2.s, qualities from 0.4 to 1.0, wall superheat from 25 to 420 K and an operating pressure of 3MPa.

The improved Dougall-Rohsenow correlation is as follows:

$$h_{DR} = 0.023 \frac{\lambda_{g,f}}{D_H} \left[\frac{D_H G}{\nu_{g,f}} \left(\frac{x_1}{\rho_{g,s}} + \frac{1 - x_1}{\rho_{l,s}} \right) \right]^{0.8} \mathrm{Pr}_{g,f}{}^{0.4} \tag{11}$$

The improved Dougall-Rohsenow correlation is developed based on operating pressures from 2-18 MPa and mass fluxes from 33 - 1,100 kg/m^2.s for multi rod geometry.

The Groeneveld correlation in the post-BT region is as follows:

$$h_G = 0.00327 \frac{\lambda_{g,s}}{D_H} \left[\frac{D_H G}{\nu_{g,s}} \left(\frac{x_1}{\rho_{g,s}} + \frac{1 - x_1}{\rho_{l,s}} \right) \right]^{0.901} \times \left[1 - 0.1 (1 - x_1)^{0.4} \left(\frac{\rho_{l,s}}{\rho_{g,s}} - 1 \right)^{0.4} \right]^{-1.5} \mathrm{Pr}_{g,w}{}^{1.32} \tag{12}$$

The Groeneveld correlation is based on a wide range of measured data that includes operating pressures from 3.5 to 21.5 MPa, mass fluxes from 690 to 5,300 kg/m^2.s, and qualities from 0.1 to 0.9 both for a tube and annulus geometry.

The Koizumi's correlations for both multi and single rod geometries agree well with the experimental data for the case of lower mass flux of 300 kg/m^2.s at an operating pressure of 2 MPa. On the other hand, the Groeneveld correlation underpredictes largely the experimental data especially in the high wall superheat region and shows slight underestimation for the low wall superheat region. The reason is that the Groeneveld correlation is valid for mass flux range of 690-5300 kg/m^2.s and extrapolation of his correlation in the low mass flux range does not work well. The improved Dougall-Rohsenow correlation predicts roughly in the high wall superheat region but it does not predict well the experimental data especially in the lower wall superheat region. The effect of mass flux on local heat transfer coefficients under the same operating pressure with **F**ig.6 (TS01) is shown in Fig.6 (TS02 and TS03). When the mass flux increases from 300 to 500 kg/m^2.s, the enhancement of local heat transfer coefficient is not found both in the high and low wall superheat regions as of Fig.6 (TS02).

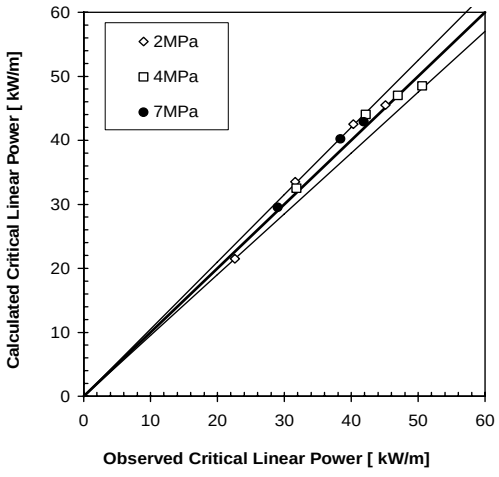

Fig 4: Observed and calculated critical linear power at preheating section

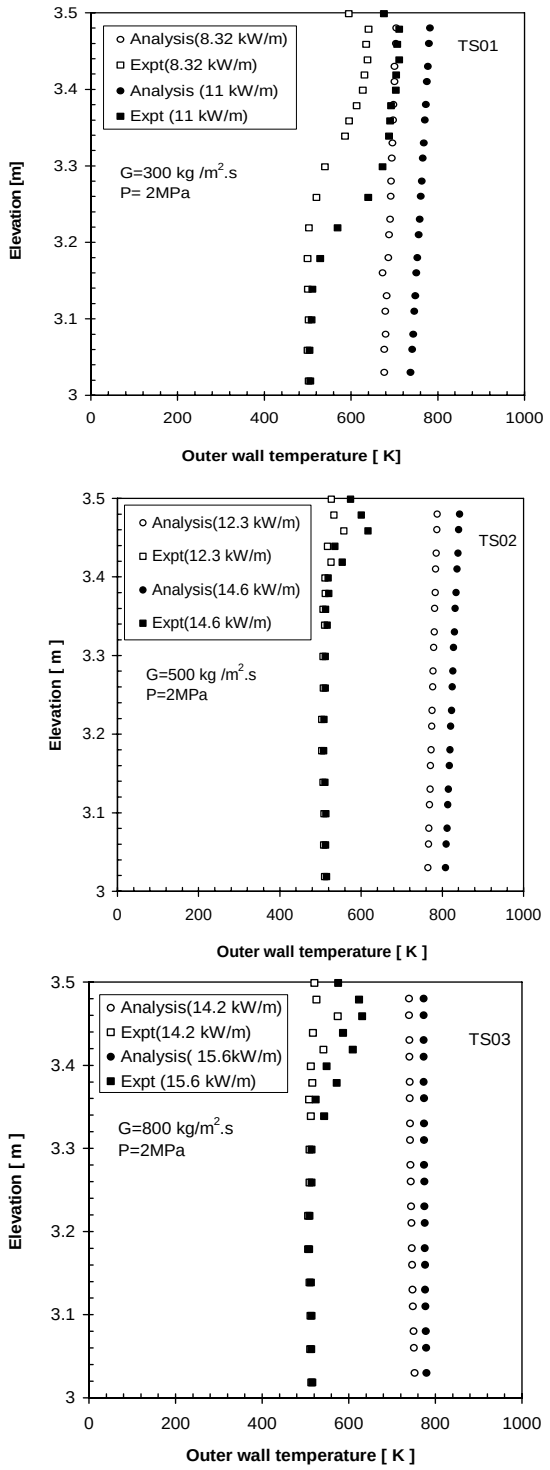

Fig 5: Comparison between calculated and measured outer wall temperature in a vertical tube with mass flux range of 300-800 kg/m^2.s at 2MPa, TS01; G=300 kg/m^2.s, TS02; G=500, kg/m^2.s, TS03; G=800 kg/m^2.s

It is also found that the agreement between the COBRA-TF analysis and experimental data shows a good predictive capability of COBRA-TF code for high wall superheat region but the Koizumi's correlation for single rod geometry shows a large overprediction over the experimental data as well as COBRA-TF analysis when the mass flux increases from 300 to 800 kg/m^2.s. This means that Koizumi's correlation for single rod geometry may not be applicable to high mass flux. However, the Koizumi's correlation for multi rod geometry roughly predicts the experimental data at higher mass fluxes although a slight poor agreement is found in the low superheat region.

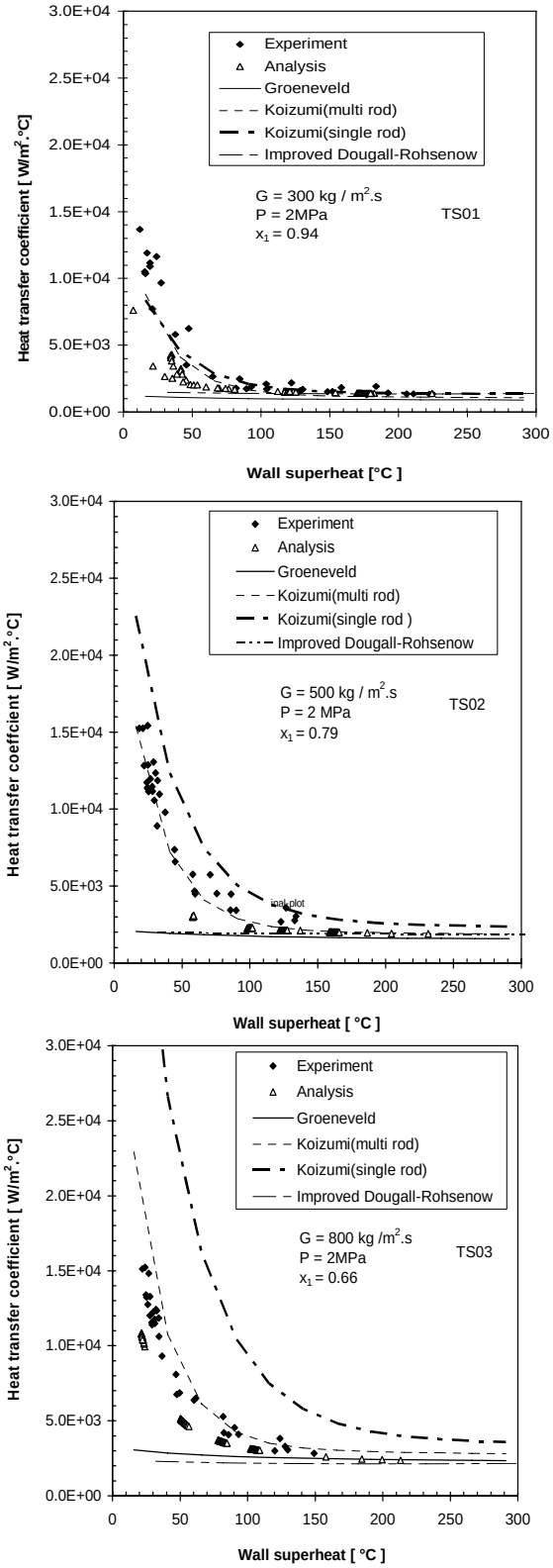

Fig 6: Variation of heat transfer coefficient on wall superheat in a vertical tube with mass flux range of 300-800 kg/m^2.s at 2MPa ,TS01; G=300 kg/m^2.s, TS02; G=500, kg/m^2.s, TS03; G=800 kg/m^2.s

5. CONCLUSIONS

Both of the experimental and numerical studies showed that the post-BT heat transfer strongly depends on the wall superheat. The local heat transfer coefficient is high in the low wall superheat region and decreases with an increase in the wall superheat asymptotically. The enhancement of heat transfer coefficient did not occur with the increase of operating pressures and mass fluxes as well. The agreement between experimental and numerical results is relatively satisfactory in the high wall superheat region compared with that of the low wall superheat region. Better estimations are to be expected by COBRA-TF code through modification of heat transfer models in the code or inclusion of suitable correlations for example, the Koizumi's correlation for multi rod geometry. The Koizumi's correlation for multi rods geometry well simulates the experimental heat transfer data in the high wall superheat condition and roughly reproduce them in low wall superheat condition. It has found that the post-BT empirical correlations based on multi rod geometry simulate well the present investigated single tube experimental data. This means that the present single tube geometrical configuration well simulates the subchannel configuration of the multi rod geometry. The improved Dougall-Rohsenow correlation roughly predicts heat transfer data in the high wall superheat region but disagreed in the low wall superheat region. The Groeneveld correlation is unable to interpret the heat transfer data due to limited range of applicability. Both the improved Dougall-Rohsenow and Groeneveld correlations shall not be extrapolated outside the recommended range. Thus, it would be a worthy step to develop a reliable correlation with insightful meaning for post-BT region under a wide range of conditions.

6. REFERENCES

1. Akiyama, M., Inoue, A., Ohishi, M., Morooka, S., Hoshide, A., Ishizuka, T., Yoshimura, K., Study of post-BT heat transfer in a full scale BWR (8×8) rod bundle, *Nucl. Eng. Des.*, 117, 341-347 (1989).
2. Groeneveld, D.C., Leung, L.K.H., Vasic, A.Z., Guo, Y.J., Cheng, S.C., A look-up table fully-developed film boiling heat transfer, *Nucl. Eng, Des*., 225, 83-978 (2003).
3. Groeneveld, D.C, Post dryout heat transfer at reactor operating conditions, AECL- 4513 (1973).
4. Groeneveld, D.C, The onset of dry sheath condition-A new definition of dryout, *Nucl. Eng. Des.*, 92, 135-140 (1986).
5. Gill, L.E., Hewitt, G.F., Hitchon, J.W., Sampling probe studies of the gas core in annular two-phase flow; Part II. Studies of the effect of phase flow rates on phase and velocity distribution, AERE-R-3955 (1963).
6. Gill, L.E., Hewitt, G.F., Hitchon, J.W., Sampling probe studies of the gas core in annular two-phase flow; Part I. The effect of length on phase and velocity distribution, AERE-R-3954 (1962).
7. Grigull, U., Sandber, H., *Heat Conduction*, Hemisphere publishing Co., 37-39 (1984).
8. Hewitt, G.F., *Handbook of Multiphase Systems*, McGraw-Hill Book Co., 10-89 (1982).
9. Hewitt, G.F., Kearsey, H.A., Keeys, R.K.F., Determination of rate of deposition of droplets in a heated tube with steam-water flow at 1000 p.s.i.a., AERE-R-6118 (1969).
10. Incropera, F.P., DeWitt D.P., Fundamentals of heat and mass transfer, 3rd. ed., John Wiley & Sons, Inc., New York, 541-544 (1990).
11. Investigation on Post-BT heat transfer in abnormal transients, METI Report (2006).
12. James J. Duderstadt and Louis J. Hamilton, Nuclear Reactor Analysis, John Wiley & Sons (1976).
13. J. M. Delhaye, M. Giot and M.L. Riethmuller, Thermohydraulics of Two-Phase Systems for Industrial Design and Nuclear Engineering, Hemisphere Publishing Corporation (1981).
14. Katto, Y., Ohno, H., An improved version of the generalized correlation of critical heat flux for the forced convection boiling in uniformly heated vertical tube, *Int. J. Heat Mass Transfer*, 27,9,1641-1648 (1984).
15. Koizumi, Y., Kumamaru, H., Yonomoto, T., Tasaka, K., Post-dryout heat transfer of high-pressure steam-water two-phase flow in single rod channel and multi rod bundle, *Nucl. Eng. Des*., 99, 157-165 (1987).
16. Lahey, R.T., Moogy, F.J., The thermal-hydraulics of a boiling water nuclear reactor, Second ed., American Nuclear Society, 124-126 (1979).
17. Milashenko, V.I., Nigmatulin, B.I., Petukhov, V.V., Trubkin, N.I., Burnout and distribution of liquid in evaporative channel of various length, *Int. J. Multiphase Flow*, 15, 393-401(1988).
18. Mesler, R.B., An alternative to the Dengler and Addoms convection concept of forced convection flow boiling heat transfer, *AIChE J*., 23, 448-453 (1977).
19. Okawa, T., Kotani, A., Kataoka, I., Naitoh, M., Prediction of the critical heat flux in annular regime in various vertical channels, *Nucl. Eng. Des.*, 229**,** 223-236 (2004).
20. Saito, T. Hughes, E.D., Carbon, M.W., Multi-fluid modeling of annular two-phase flow, *Nucl. Eng. Des*., 50, 225-271(1978).
21. Sun, G., Hewitt, G.F., Evaporation and condensation of steam-water in a vertical tube, *Nucl. Eng. Des*., 207, 137-145 (2001).
22. Standard for Assessment of Fuel Integrity under Anticipated Operational Occurrences in BWR Power Plants, AESJ-SC-P002 (2003).
23. Todreas, Neil E. and Mazzini, Majid S., Nuclear Systems I, Thermal-hydraulic Fundamentals, Taylor & Francis, Second Edition (1993).
24. Ueda, T., Isayama, Y., Critical heat flux and exit film flow rate in a flow boiling system, *Int. J. Heat Mass Transfer*, 24, 1267-.1276 (1981).